Multichannel Seismic Deconvolution Using Markov–Bernoulli Random-Field Modeling

Alon Heimer and Israel Cohen, *Senior Member, IEEE*

***Abstract*—In this paper, we present an algorithm for multichannel blind deconvolution of seismic signals, which exploits lateral continuity of Earth layers based on Markov–Bernoulli random-field modeling. The reflectivity model accounts for layer discontinuities resulting from splitting, merging, starting, or terminating layers within the region of interest. We define a set of reflectivity states and legal transitions between the reflector configurations of adjacent traces and subsequently apply the Viterbi algorithm for finding the most likely sequences of reflectors that are connected across the traces by legal transitions. The improved performance of the proposed algorithm and its robustness to noise, compared with a competitive algorithm, are demonstrated using simulated and real seismic data examples, in blind and nonblind scenarios.**

***Index Terms*—Multichannel deconvolution, reflectivity estimation, seismic signal, sparse reflectivity, wavelet estimation.**

I. Introduction

In SEISMIC exploration, a short-duration seismic pulse is transmitted from the surface, reflected from boundaries between underground Earth layers, and received by an array of sensors on the surface. The received signals, called seismic traces, are analyzed to extract information about the underground structure of the layers in the explored area [1], [2]. Preprocessing is applied to the raw data in order to increase the signal-to-noise ratio (SNR) and attenuate surface waves that are unrelated to the underground structure. Subsequently, the traces can be modeled under simplifying assumptions as noisy outcomes of convolutions between reflectivity sequences (channels) and a certain wavelet. The objective of multichannel seismic deconvolution is to estimate the reflectivity sequences from the measured traces and, in the blind case, also to estimate the unknown wavelet.

Nonblind deconvolution is clearly simpler than blind deconvolution; however, both suffer from sensitivity to noise due to the ill-conditioned nature of the problem. In order to cope with this sensitivity, some model of the reflectivity and wavelet is often utilized. Mendel *et al.* [3] assume an autoregressive moving-average model and use a maximum likelihood estimator for the reflectivity. Baziw and Ulrych [4] model the overlapping wavelets in the received signal as amplitude-modulated sinusoids and use particle filtering to separate them. Kaaresen and Taxt [5] assume that the wavelet is of short duration, and Santamaria *et al.* [6] use a Gaussian mixture model for the reflectivity sequence. While statistical methods generally require a large data set for derivation of a good estimate [7]–[9], sparsity of the reflectivity sequences can be exploited to cope with the ill-posed nature of the basic blind deconvolution problem [5], [10] and to improve the performance of nonblind deconvolution methods [11]. Channel sparsity enables efficient channel estimation, which is suitable for relatively short traces [5], [12].

Multichannel blind deconvolution (see [13] and references therein, [14], and [15]) is often more advantageous and more robust than single-channel blind deconvolution. Certain relations between spatially near channels are used to regularize the problem. Lateral continuity of the reflectors across channels has been used in [5] to further improve the channel estimates (see also [16]). Idier and Goussard [17] model the 2-D structure of the underground reflectivity as a Markov–Bernoulli random field and impose lateral continuity to generate deconvolution results that are superior to those obtainable by single-channel deconvolution methods. However, since the parametric models used in these works result in a nonconvex optimization problem, a global optimal solution is very difficult to achieve. Usually, some sort of constrained search is performed within a group of possible solutions for the locations of reflectors (such as the single most likely replacement (SMLR) approach in [18]), and a typical tradeoff remains between the extent of the search, the computational complexity, and the optimality of the final solution. Lavielle [19] has modeled the 2-D reflectivity as a Markov random field and used simulated annealing and a maximum *a posteriori* probability (MAP) criterion for its estimation. Rosec, Boucher, Nsiri, and Chonavel use the Monte Carlo Markov chain and the Gipps sampler to generate samples of the reflectivity according to its posterior distribution and estimate it by averaging over them.

Recently, we have proposed a deconvolution method that attempts to maximize a MAP criterion using dynamic programming [20], [21]. A search is performed among continuous paths of reflectors instead of single reflectors, and the best continuous reflector paths are chosen by dynamic programming. We showed that our approach recovers the reflectivity better than the iterative windowed maximization (IWM) algorithm [5] and, particularly, its advantage is more significant when the SNR is low. However, our reflectivity model did not take into account layer discontinuities. As a result, the application of our algorithm was limited to areas of mostly continuous layers.

Manuscript received April 17, 2008; revised September 19, 2008 and December 7, 2008. First published April 10, 2009; current version published June 19, 2009.

The authors are with the Department of Electrical Engineering, Technion—Israel Institute of Technology, Haifa 32000, Israel (e-mail: heimer@tx.technion.ac.il; icohen@ee.technion.ac.il).

Color versions of one or more of the figures in this paper are available online at http://ieeexplore.ieee.org.

Digital Object Identifier 10.1109/TGRS.2008.2012348

In this paper, we introduce an improved method for estimating the 2-D reflectivity pattern by using a Markov–Bernoulli random-field modeling. Unlike the model proposed in [20] and [21], the Markov–Bernoulli random field accounts for layer discontinuities resulting from splitting, merging, starting, or terminating layers within the region of interest. The algorithm performs a search only among a subgroup of 2-D reflectivity patterns that fit into the model. The Viterbi algorithm [22] is employed for efficiently finding the most likely reflectivity pattern at each iteration. We define a set of reflectivity states and legal transitions between reflector configurations of adjacent traces and subsequently extract sequences of reflectors across the traces, connected by legal transitions with the highest likelihood. The performance of the proposed algorithm is investigated for reflectivity patterns that contain discontinuities. Improved performance and robustness to noise are demonstrated for simulated and real seismic data in blind and nonblind scenarios. The rest of this paper is organized as follows. In Section II, we describe the signal and reflectivity model. In Section III, we present a relaxed optimization criterion for deconvolution and incorporate the Viterbi algorithm in the optimization procedure. In Section IV, we demonstrate the improved performance of the proposed algorithm compared with an existing algorithm, using simulated and real seismic data. Finally, we conclude in Section V and discuss the additional complexity of the proposed algorithm.

II. Signal Model

A. Signal Model

We assume M received signals (traces) $z^{(m)}[n]$ of length $N+K-1$, each generated by a single input signal $h[n]$ of length K passing through a channel $x^{(m)}[n]$ of length N, which represents the reflectivity sequence of the mth trace. The output signal of channel m can be written as

$$z^{(m)}[n] = \sum_{k=0}^{K-1} h[k]x^{(m)}[n-k] + e^{(m)}[n] \qquad (1)$$

for $m = 1, \ldots, M$ and $n = 1, \ldots, N+K-1$, where $e^{(m)}[n]$ denotes white Gaussian noise, which is statistically independent of the reflectivity sequence $x^{(m)}[n]$ and $h[n]$. We denote by $\mathbf{z}_m \in \boldsymbol{R}^{N+K-1}$ the observation vector of a single trace m and by $\mathbf{z} \in \boldsymbol{R}^{(N+K-1)\times M}$ the matrix of observations, which is the concatenation of the vectors $\mathbf{z}_m$, $m = 1, \ldots, M$, as columns.

B. Reflectivity Model

1) Geometric Field: Let $\mathbf{x} \in \boldsymbol{R}^{N\times M}$ represent the 2-D reflectivity pattern, and let $\mathbf{q} \in \{0,1\}^{N\times M}$ denote a binary matrix representing the existence of reflectors in $\mathbf{x}$, i.e., $q\,(n,m) = 1$ if there is a reflector in row n and column m of $\mathbf{x}$; otherwise, $q\ (n,m) = 0$. Let $\mathbf{t}^{/}$, $\mathbf{t}^{-}$, and $\mathbf{t}^{\backslash} \in \{0,1\}^{N\times M}$ be binary matrices representing transition variables of reflectors in $\mathbf{x}$ for ascending, horizontal, and descending layers, respectively, i.e., $t^{/}(n,m) = 1$ if $q\ (n,m) = q\ (n-1, m+1) = 1$, and these two reflectors belong to the same layer boundary; otherwise, $t^{/}(n,m) = 0$. In a similar way, $t^{-}(n,m) = 1$ if $q\ (n,m) = q\ (n,m+1) = 1$, and these two reflectors belong to the same layer boundary; otherwise, $t^{-}(n,m) = 0$. Moreover, $t^{\backslash}(n,m) = 1$ if $q\ (n,m) = q\ (n+1, m+1) = 1$, and these two reflectors belong to the same layer boundary; otherwise, $t^{\backslash}(n,m) = 0$. Using these definitions, the 2-D reflectivity model is defined as follows.

1) For each column m, the sequences $\{t^{/}(n,m)\}_n$, $\{t^{-}(n,m)\}_n$, and $\{t^{\backslash}(n,m)\}_n$ are white binary processes.
2) For each column m, the sequence $\{q\ (n,m)\}_n$ is a white binary process.
3) $p\{t^{/}(n,m), t^{-}(n,m), t^{\backslash}(n,m)\} = p\{t^{/}(n,\ m)\}p\{t^{-}(n,\ m)\}p\{t^{\backslash}(n,m)\}$.
4) $p\{t^{/}(n,m-1) = a, t^{-}(n,m-1) = b, t^{\backslash}(n,m-1) = c, q\ (n,m)\} = p\{t^{/}(n,m) = a, t^{-}(n,m) = b, t^{\backslash}(n,m) = c, q\ (n,m)\}$.
5) $p\{t^{/}(n,m-1) = 0, t^{-}(n,m-1) = 0, t^{\backslash}(n,m-1) = 0 | q\ (n,m) = 0\} = 1$.
6) $\forall n,m$: $p\{t^{/}(n,m) = 1\} = \mu^{/}$, $p\{t^{-}(n,m) = 1\} = \mu^{-}$, $p\{t^{\backslash}(n,m) = 1\} = \mu^{\backslash}$.
7) $\forall n,m$: $p\{q\ (n,m) = 1\} = \lambda$.
8) $\forall n,m$: $p\{q\ (n,m) = 1 | t^{/}(n+1,m-1) = 0, t^{-}(n,m-1) = 0, t^{\backslash}(n-1,m-1) = 0\} = \varepsilon$.

Properties 6), 7), and 8) define the parameters of the geometric model $\mu^{/}$, μ^{-}, $\mu^{\backslash}$, λ, and ε, which are related by $\lambda = 1 - (1-\mu^{/})(1-\mu^{-})(1-\mu^{\backslash})(1-\varepsilon)$.

2) Amplitude Field: The amplitude field of the reflectivity pattern is characterized by two parameters r and σ_a^2. A reflector in $x\ (n_1, m-1)$ is said to be a predecessor of a reflector in $x\ (n_2, m)$ [or $x\ (n_2, m)$ is said to be a successor of $x\ (n_1, m-1)$] if $q\ (n_1, m-1) = 1$, $q\ (n_2, m) = 1$, $|n_1 - n_2| \le 1$, and the transition variable connecting these two reflectors is equal to one. Then, the amplitude field is defined as follows.

9) If there is no reflector in $x\ (n_2, m)$, then $x\ (n_2, m) = 0$.
10) If there is a reflector in $x\ (n_2, m)$, which has no predecessors, then $x\ (n_2, m) \sim N(0, \sigma_a^2)$.
11) If there is a reflector in $x\ (n_2, m)$, which is a distinct successor of a particular predecessor $x\ (n_1, m-1)$, then $x\ (n_2, m) \sim N(rx(n_1, m-1), (1-r^2)\sigma_a^2)$.
12) If there is a reflector in $x\ (n_2, m)$, which has more than one predecessor or is not a distinct successor of a particular reflector, then $x\ (n_2, m) \sim N(0, \sigma_a^2)$.

It is shown in [17] and [23] that these definitions describe a Markov–Bernoulli random field of reflectors with Gaussian amplitudes, which is homogenous and symmetric. In each column, the binary variable representing the existence of a reflector is Bernoulli distributed with the parameter λ. The probability of a new boundary appearing or disappearing at a certain sample is ε, and the parameters $\mu^{/}$, μ^{-}, $\mu^{\backslash}$, and ε determine the degree of geometric continuity of layer boundaries. The amplitudes of reflectors in a single column form a white sequence. The parameter σ_a^2 determines the variance of the amplitudes, and the parameter r determines the degree of continuity of amplitudes along a layer boundary. Fig. 1 shows some examples of 2-D

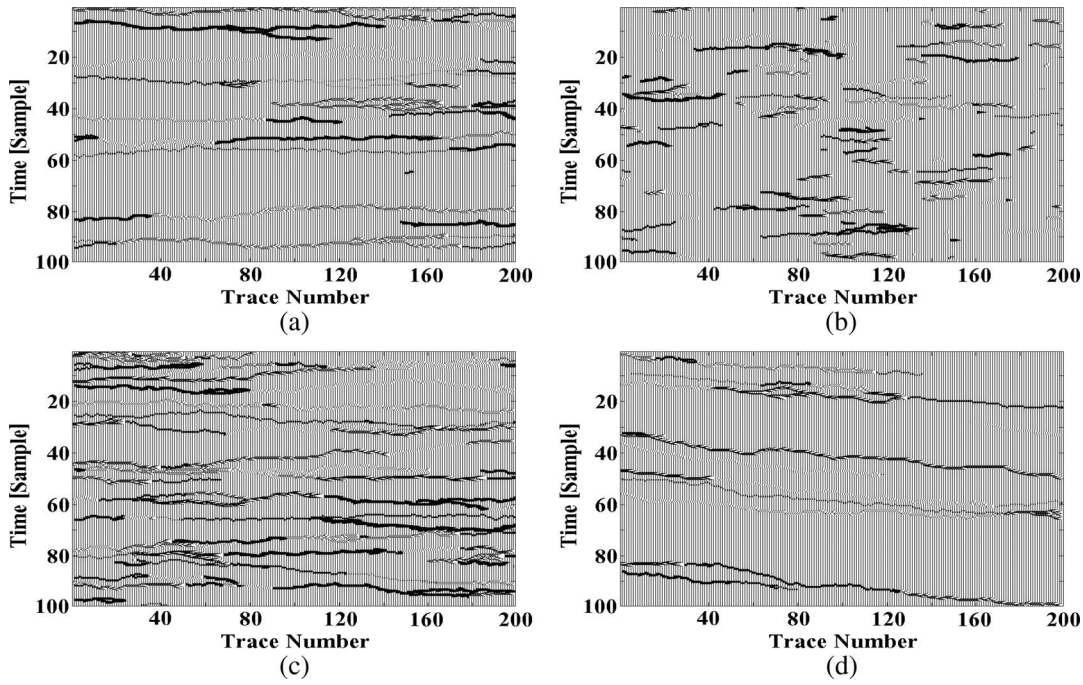

Fig. 1. Two-dimensional reflectivity patterns generated with various parameters values.

TABLE I
PARAMETERS USED FOR GENERATING 2-D REFLECTIVITY PATTERNS

	λ	ϵ	$\mu^{/}$	μ^{-}	$\mu^{\backslash}$	r
1(a)	0.05	0.0001	0.0084	0.0335	0.0084	1.0
1(b)	0.053	0.0003	0.0084	0.0335	0.0084	1.0
1(c)	0.099	0.0001	0.0168	0.067	0.0168	1.0
1(d)	0.05	0.0001	0.0044	0.0335	0.0124	1.0

reflectivity patterns generated by this model with different parameters. The parameters' values used to generate these patterns are shown in Table I.

III. ESTIMATION PROCEDURE

A. MAP Estimation

Let $\mathbf{x}_m$ and $\mathbf{q}_m$ be the mth columns of the matrices $\mathbf{x}$ and $\mathbf{q}$, respectively, and let $\mathbf{a}_m$ denote the amplitudes of reflectors in the reflectivity sequence $\mathbf{x}_m$. Note that the size of $\mathbf{a}_m$ may vary for different m's according to the number of reflectors in the specific column m. We would like to perform a maximum *a posteriori* estimation of the locations and amplitudes of reflectors given the observations

$$\{\widehat{\mathbf{q}}, \widehat{\mathbf{a}}\} = \arg\max p(\mathbf{q}, \mathbf{a}|\mathbf{z}). \tag{2}$$

Using Bayes' rule, we have $p(\mathbf{q}, \mathbf{a}|\mathbf{z}) = p(\mathbf{z}|\mathbf{q}, \mathbf{a})p(\mathbf{a}|\mathbf{q})p(\mathbf{q})/p(\mathbf{z})$. According to the reflectivity model, the sequences $\{\mathbf{q}_m|m = 1, \ldots, M\}$ and $\{\mathbf{a}_m|m = 1, \ldots, M\}$ are vector Markov processes of the first order, i.e., $p(\mathbf{q}_m|\mathbf{q}_{m-1}, \ldots, \mathbf{q}_1) = p(\mathbf{q}_m|\mathbf{q}_{m-1})$, and $p(\mathbf{a}_m|\mathbf{q}_m, \ldots, \mathbf{q}_1, \mathbf{a}_{m-1}, \ldots, \mathbf{a}_1) = p(\mathbf{a}_m|\mathbf{q}_m, \mathbf{q}_{m-1}, \mathbf{a}_{m-1})$. Accordingly, (2) can be rewritten as

$$\begin{aligned}\{\widehat{\mathbf{q}}_1, \ldots, \widehat{\mathbf{q}}_M, \widehat{\mathbf{a}}_1, \ldots, \widehat{\mathbf{a}}_M\} &= \underset{\mathbf{q}_1,\ldots,\mathbf{q}_M,\mathbf{a}_1,\ldots,\mathbf{a}_M}{\arg\max} \Bigg\{ p(\mathbf{z}_1|\mathbf{q}_1, \mathbf{a}_1)p(\mathbf{a}_1|\mathbf{q}_1)p(\mathbf{q}_1) \\ &\quad \times \prod_{m=2}^{M} p(\mathbf{z}_m|\mathbf{q}_m, \mathbf{a}_m) \\ &\quad \times p(\mathbf{a}_m|\mathbf{q}_m, \mathbf{q}_{m-1}, \mathbf{a}_{m-1}) \\ &\quad \times p(\mathbf{q}_m|\mathbf{q}_{m-1}) \Bigg\}. \end{aligned} \tag{3}$$

B. Suboptimal Estimation

Let $\widehat{\mathbf{x}}^t$ and $\widehat{\mathbf{q}}^t$ denote estimates of $\mathbf{x}$ and $\mathbf{q}$, respectively, in iteration t. Let $\widehat{\mathbf{q}}_m^{t,n}$ represent the column m of the matrix $\widehat{\mathbf{q}}^t$, with the insertion of a new reflector in line n. Let $\widehat{\mathbf{a}}(\widehat{\mathbf{q}}_m^{t,n})$ denote an estimate of the reflectors' amplitudes in $\widehat{\mathbf{q}}_m^{t,n}$, given the observation $\mathbf{z}_m$. We define the following set of states and legal transitions to which we will refer as the states set, as shown in Fig. 2. Each column m in the states set consists of possible configurations of reflectors in the mth column in the reflectivity estimate and the amplitudes' estimates associated with them. The first N states in each column describe reflector configurations that have a single additional reflector in the nth line with respect to the current estimate (if there is already a reflector in that line in the current estimate, then there is no change). The last state in each column describes a reflector configuration that is identical to that of the current estimate. Legal transitions denoted by black arrows exist from each

of the first N states in a column to the three closest states in the next column, i.e., the states in the next column that are in the previous, the same, and the next lines. In addition, legal transitions exist from each of the first N states in a column to the last state in the next column and from the last state in a column to each of the first N states in the next column. A legal path is a sequence of M states, one from each column of the states set, for which there are legal transitions from each state in the path to the next one. Let us denote, as s_m, a chosen state from column m of the states set. We define the maximum *a posteriori* estimated path as follows:

$$\{\widehat{s}_1, \ldots, \widehat{s}_M\} = \underset{\{s_1,\ldots,s_M\}\in\{\text{Legal Paths}\}}{\arg\max} p(s_1, \ldots, s_M|\mathbf{z}_1, \ldots, \mathbf{z}_M). \quad (4)$$

We denote by n_m the line in the states set from which s_m is taken. Now, explicitly formulating (4), we obtain (5), shown at the bottom of the page. Comparing (3) and (5), we can observe three differences that make the latter suboptimal. The first is the fact that the target function is maximized only over the set of reflector configurations defined by the states set. These configurations are formed by slightly altering the configurations in the current estimate and, hence, do not include all configurations. However, an iterative procedure, as will be presented later, helps to overcome this limitation. In addition, not all paths in the states set are legal by our somewhat arbitrary definition of legal transitions; hence, some 2-D configurations are not examined. However, the states set and the definition of the legal transitions are designed so that it well represents the nature of the reflectors' patterns as described by the 2-D reflectivity model, since most layer boundaries are represented by legal paths in the states set. The last difference is that the maximization is not performed simultaneously for $\mathbf{q}$ and $\mathbf{a}$. Instead, a preceding step of estimating $\widehat{\mathbf{a}}(\mathbf{q}_m^{t,n})$ for each $\mathbf{q}_m^{t,n}$ is performed and, subsequently, the maximization of (5). Notice that the state set was designed so that a legal path of states represents a quasi-continuous boundary. When a chosen path goes through states in the last line of states, this means that no new reflectors are added in these columns; hence, there is a discontinuity in the added boundary. In [20] and [21], the examined boundaries all started at the first column and ended at the last; hence, no discontinuities were possible, and the algorithm could recover, less efficiently, the reflectivity of underground sections that contained such discontinuities.

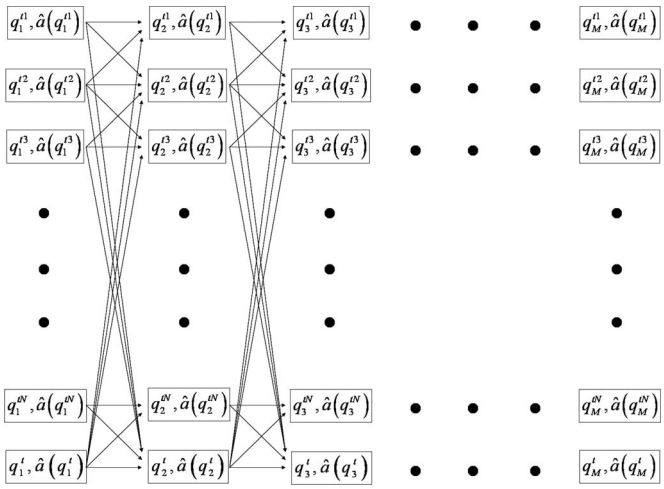

Fig. 2. Illustration of states and legal transitions for a single iteration of the estimation procedure.

C. Estimation Procedure

In [17], the maximization of a suboptimal MAP criterion is performed iteratively, where, in each iteration, the reflectivity of a single column is estimated, given the estimated locations and amplitudes of the reflectors in the previous column. In other words, the estimation of the reflectivity of all previous columns is held fixed, while the posterior probability of the current column's reflectivity is maximized given all previous columns. This approach is suboptimal, as explained in [17]. The advantage of the approach presented in this paper is that the reflectivity of a column is not determined before all columns are examined and that the 2-D criterion (5) is hence truly globally maximized in an optimal way, as will be explained (although this criterion itself is a suboptimal 2-D criterion, as explained in the previous section). The fact that the location of reflectors is not determined until all columns are scanned forces us to estimate the amplitudes for each examined configuration of

$$\begin{aligned}
&\left\{\widehat{\mathbf{q}}_1^{t+1}, \widehat{\mathbf{a}}\left(\widehat{\mathbf{q}}_1^{t+1}\right), \ldots, \widehat{\mathbf{q}}_M^{t+1}, \widehat{\mathbf{a}}\left(\widehat{\mathbf{q}}_M^{t+1}\right)\right\} \\
&= \underset{\{n_1,\ldots,n_M\}\in\{\text{Legal Paths}\}}{\arg\max} p\left\{\mathbf{q}_1^{t,n_1}, \widehat{\mathbf{a}}\left(\mathbf{q}_1^{t,n_1}\right), \ldots, \mathbf{q}_M^{t,n_M}, \widehat{\mathbf{a}}\left(\mathbf{q}_M^{t,n_M}\right)|\mathbf{z}_1, \ldots, \mathbf{z}_M\right\} \\
&= \underset{\{n_1,\ldots,n_M\}\in\{\text{Legal Paths}\}}{\arg\max} p\left\{\mathbf{z}_1, \ldots, \mathbf{z}_M|\mathbf{q}_1^{t,n_1}, \widehat{\mathbf{a}}\left(\mathbf{q}_1^{t,n_1}\right), \ldots, \mathbf{q}_M^{t,n_M}, \widehat{\mathbf{a}}\left(\mathbf{q}_M^{t,n_M}\right)\right\} \\
&\quad \times p\left\{\mathbf{q}_1^{t,n_1}, \widehat{\mathbf{a}}\left(\mathbf{q}_1^{t,n_1}\right), \ldots, \mathbf{q}_M^{t,n_M}, \widehat{\mathbf{a}}\left(\mathbf{q}_M^{t,n_M}\right)\right\} \\
&= \underset{\{n_1,\ldots,n_M\}\in\{\text{Legal Paths}\}}{\arg\max} p\left\{\mathbf{z}_1|\mathbf{q}_1^{t,n_1}, \widehat{\mathbf{a}}\left(\mathbf{q}_1^{t,n_1}\right)\right\} p\left\{\widehat{\mathbf{a}}\left(\mathbf{q}_1^{t,n_1}\right)|\mathbf{q}_1^{t,n_1}\right\} p\left\{\mathbf{q}_1^{t,n_1}\right\} \\
&\quad \times \prod_{m=2}^{M} p\left\{\mathbf{z}_m|\mathbf{q}_m^{t,n_m}, \widehat{\mathbf{a}}\left(\mathbf{q}_m^{t,n_m}\right)\right\} p\left\{\widehat{\mathbf{a}}\left(\mathbf{q}_m^{t,n_m}\right)|\mathbf{q}_m^{t,n_m}, \mathbf{q}_{m-1}^{t,n_{m-1}}, \widehat{\mathbf{a}}\left(\mathbf{q}_{m-1}^{t,n_{m-1}}\right)\right\} p\left\{\mathbf{q}_m^{t,n_m}|\mathbf{q}_{m-1}^{t,n_{m-1}}\right\} \quad (5)
\end{aligned}$$

reflectors in a column, regardless of adjacent columns (whose reflectors' locations are not yet known). Hence, as mentioned in the previous section, a preceding step of estimating $\widehat{\mathbf{a}}(\mathbf{q}_m^{t,n})$ for each $\mathbf{q}_m^{t,n}$ in the states set is performed before (5) is maximized. In this paper, a maximum *a posteriori* estimator is used for this estimation

$$\widehat{\mathbf{a}}(\mathbf{q}_m) = \arg\max_{\mathbf{a}} p(\mathbf{a}_m|\mathbf{q}_m, \mathbf{z}_m). \tag{6}$$

Using a matrix form of (1), i.e., $\mathbf{z}_m = \mathbf{H}_{\mathbf{q}_m}\mathbf{a}_m + \mathbf{e}_m$, where $\mathbf{H}_{\mathbf{q}_m}$ is composed of replicas of h translated to the locations of reflectors, we have $\mathbf{z}_m|\mathbf{q}_m$, $\mathbf{a}_m \sim N(\mathbf{H}_{\mathbf{q}_m}\mathbf{a}_m, \sigma_e^2\mathbf{I})$, and $\mathbf{a}_m|\mathbf{q}_m \sim N(\mathbf{0}, \sigma_a^2\mathbf{I})$. Accordingly, (6) yields the following known estimator:

$$\widehat{\mathbf{a}}(\mathbf{q}_m) = \left(\mathbf{H}_{\mathbf{q}_m}^{\mathrm{T}}\mathbf{H}_{\mathbf{q}_m} + \frac{\sigma_e^2}{\sigma_a^2}\mathbf{I}\right)^{-1}\mathbf{H}_{\mathbf{q}_m}^{\mathrm{T}}\mathbf{z}_m. \tag{7}$$

Criterion (5) is maximized using the Viterbi algorithm, as will now be described. Let $s_{n_m,m}$ denote the state in line n_m and column mth of the states set. Let $P_{n_m,m}$ be a sequence of states ("a path"), one from each column in the range $[1,\ldots,m]$ of the states set that ends with the state $s_{n_m,m}$. Let $D(P) \triangleq p(P|\mathbf{z})$ be the probability of the states in the path P given the observations $\mathbf{z}$. If the path P is composed of the states $\{s_{n_1,1},\ldots,s_{n_m,m}\}$, then we can explicitly write $D(P) = p(s_{n_1,1},\ldots,s_{n_m,m}|\mathbf{z}_1,\ldots,\mathbf{z}_m)$. Let $P^o_{n_m,m} \triangleq \arg\max_{P_{n_m,m}} D(P_{n_m,m})$ be the path that ends with the state $s_{n_m,m}$, whose probability, given the observations, is maximal. Let $B_{n_m,m}$ be the group of states from which there is a legal transition to the state $s_{n_m,m}$ in the states set. Recalling that the sequences $\mathbf{q}_m$ and $\mathbf{a}_m$ are Markov processes of the first order, we define

$$n^o_{m-1} \triangleq \arg\max_{n_{m-1}\in B_{n_m,m}} D\left(P^o_{n_{m-1},m-1}\right) \times \frac{p(\mathbf{z}_m|s_{n_m,m})p(s_{n_m,m}|s_{n_{m-1},m-1})}{p(\mathbf{z})}. \tag{8}$$

It can be shown that

$$P^o_{n_m,m} = \left(P^o_{n^o_{m-1},m-1}\vdots s_{n_m,m}\right) \tag{9}$$

where $\vdots$ describes the concatenation of the state on its right to the path on its left. Equations (8) and (9) provide an efficient way for calculating the sequence of states in the states set whose probability, given the observations, is maximal. We initialize $P^o_{n_1,1} \triangleq s_{n_1,1}$ for $n_1 = 1,\ldots,N$ and use (8) and (9) to recursively calculate $P^o_{n_M,M}$, $n_M = 1,\ldots,N$. Finally, we choose

$$n^o_M \triangleq \arg\max_{n_M} D\left(P^o_{n_M,M}\right)$$

and obtain the final desired path

$$P^o \triangleq P^o_{n^o_M,M}.$$

Notice that, in order to avoid dealing with the transition variables and to be able to calculate $p\{\mathbf{q}_m^{t,n_m}|\mathbf{q}_{m-1}^{t,n_{m-1}}\}$ in (5), we make the following approximated assumption. Whenever $\mathbf{q}(n_1, m-1) = 1$ and $\mathbf{q}(n_2, m) = 1$ and $|n_1 - n_2| \le 1$, we assume that there is a transition variable equal to one between these two reflectors. In other words, if two reflectors are in adjacent columns and in adjacent rows or in the same row, we assume that they belong to the same boundary. This approximation is very precise when λ and ε are small enough. Under this assumption, a given configuration of reflectors determines completely the value of all transition variables $\mathbf{t}^{\backslash}$, $\mathbf{t}^{-}$, $\mathbf{t}^{/}$. Given reflectors' configurations in two adjacent columns, the transition variables between these two columns, and the amplitudes estimate of reflectors in the first of these two columns, the amplitude distribution of each reflector in the second column can be determined according to properties 9)–12) of the amplitude field model.

D. Complete Algorithm Structure

When maximizing the estimation criterion by iteratively examining alternatives to the current reflectivity estimate, the optimality of the final estimate depends on the set of rules used to select the examined alternatives. It is suggested, in [5] for a single-channel deconvolution, that attempting not only to add or delete a reflector but also to change the location of a reflector has an advantage considering the overall effect on computational complexity and optimality of the final solution. Considering this result, we now describe a simple mechanism that allows not only the addition of a sequence of reflectors but also moving a sequence to a different location.

We define a "Section" of reflectors as a sequence of reflector locations $\{(n_m, m)\}_{m=m1}^{m2}$, for which $|n_m - n_{m-1}| \le 1$ for $m = m1+1,\ldots,m2$.

Each legal path selected from the states set is composed of sections of reflectors separated by columns from which the last state was selected. When we add reflectors to the estimate according to a selected path, we actually add reflectors in locations defined by these sections. We keep track of the sections that are added to the estimate in the following way. When we add a section, we try to concatenate the added section to existing sections in the estimate. Let (n_{m_1}, m_1) and (n_{m_2}, m_2) denote the location of the first and last reflectors in the added section, respectively. If there exists a unique section in the estimate whose last reflector is in location $(n_{m_1-1}, m_1 - 1)$ such that $|n_{m_1-1} - n_{m_1}| \le 1$, then we concatenate the two sections as follows. Let (n_{m_b}, m_b) be the starting reflector of the existing section; then, the description of the existing section is changed to include the reflectors of the newly added section, hence creating a section starting at (n_{m_b}, m_b) and ending at (n_{m_2}, m_2). A similar operation is performed if there is a unique section in the estimate, which starts with a reflector at location $(n_{m_2+1}, m_2 + 1)$ such that $|n_{m_2+1} - n_{m_2}| \le 1$. In this case, we concatenate the section by including the reflectors of the added section in the description of the existing section, creating a concatenated section starting at (n_{m_1}, m_1) and ending at (n_{m_c}, m_c), where (n_{m_c}, m_c) is the ending reflector of the existing section. If both situations occur, both concatenation

operations are performed, creating a section starting at (n_{m_b}, m_b) and ending at (n_{m_c}, m_c). Each time a section is added to the estimate, its description is also inserted to a list of existing sections. If an added section is concatenated with an existing one, the section with which it was concatenated is removed from the list, and the concatenated section is inserted at the end of the list. This mechanism allows us to perform some sort of sections management in order to relocate sections of reflectors. The complete structure of the algorithm is as follows.

1) Start with the empty reflectivity estimate, i.e., matrices $\widehat{\mathbf{q}}$ and $\widehat{\mathbf{x}}$ that are all zeros.
2) If there are any reflectors in the estimate, remove a section of reflectors from the estimate and from the beginning of the list of sections.
3) Define the states set, and estimate the amplitudes for each state.
4) Using a single execution of the Viterbi algorithm, find the path of states with the highest probability in the states set.
5) Insert the sections of reflectors as described by the selected path to the estimate with the proper amplitudes.
6) Insert the sections of reflectors in the selected path to the end of the list of sections performing concatenation operations, if needed.
7) Return to step 2) for the next iteration.

Step 2) is skipped during the first several iterations in order to let the estimate gather some sections of reflectors. The process is continued until no change occurs in the reflectivity estimate during a complete scan of the list of sections or until a predetermined number of iterations were performed. Notice that the number of sections of reflectors can change during the execution of the algorithm since the path of reflectors found in Step 4) can contain more than one section and Step 6) can reduce the number of sections by concatenation operations. In the rest of this paper, we refer to this algorithm as a Markov–Bernoulli deconvolution (MBD).

Although the model accounts for discontinuities, the strength of the algorithm is in exploiting the continuity; hence, regions with highly discontinuous reflectivity patterns will obviously be recovered with less accuracy. Once a discontinuity occurs, e.g., a boundary shift of more than one pixel, the amount of shift between the boundaries on both sides should not affect the results. Small discontinuities in the sampled data, which can occur in boundaries with a higher slope, can be allowed by altering the legal transitions in the state set and adding transitions between states that are further apart. Such a change, however, will result in an increased complexity.

E. Discussion on Convergence

We now provide a proof of convergence in the nonblind case. The probability of a legal path in the state set is actually the probability of the reflectivity pattern it represents given the data, as shown on the right-hand side of (5). In each iteration of the algorithm, we first remove an existing section of reflectors from the reflectivity estimate, as described in the previous section, and then, we select the legal path with the highest probability given the data among the examined set of legal paths. The reflectivity patterns described by this examined set of legal paths obviously include the reflectivity estimate that we had before removing the section of reflectors (the path that recovers this reflectivity estimate is composed of the $N+1$ state for columns that are not a part of the removed section and from the state in the line from which a reflector was removed, for each column that is a part of the removed section). Hence, by choosing the path with a maximum probability, while considering also the previous reflectivity estimate, we assure that the probability of the reflectivity estimate is greater or equal to the previous one, causing this probability to be a nondecreasing function of the iteration number. Since there is only a finite number (although very large) of reflectivity patterns, this probability is also bounded and, therefore, converges, which is the same for the reflectivity estimate. In all executions of the algorithm however, the convergence was much faster than is implied by this very loose bound, usually after a few dozen iterations. A typical graph of the convergence of probability function is shown in Fig. 3. The convergence in the blind case is less easy to prove, since between iterations, the wavelet estimate also changes; hence, although we also consider the previous

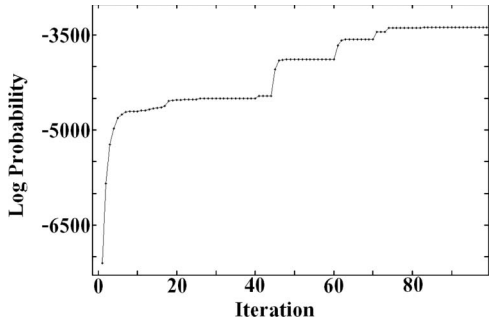

Fig. 3. Typical convergence of the posterior log probability of the reflectivity estimate for 130 × 130 data in a nonblind case.

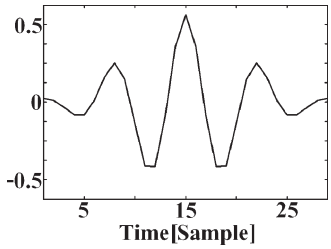

Fig. 4. Wavelet used in the simulated examples.

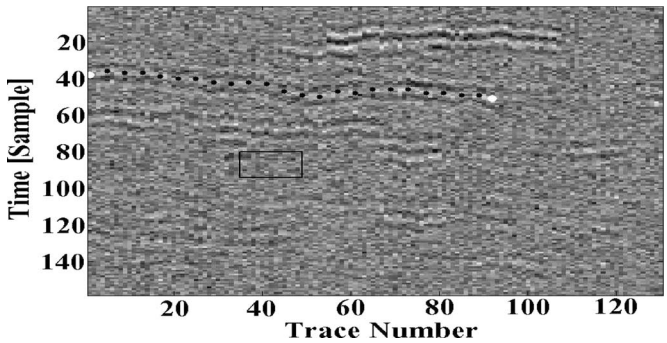

Fig. 5. Estimating the noise variance and $\mu^{/}$, μ^{-}, and $\mu^{\backslash}$ from the data.

TABLE II
TRUE AND ESTIMATED VALUES OF PARAMETERS USED FOR NONBLIND DECONVOLUTION EXAMPLES

		Example 1: SNR -5dB			Example 2: SNR 0dB	
Parameter	True Value	Estimates		True Value	Estimates	
		Execution: 1	2		Execution: 1	2
r	1.0	1.0	1.0	1.0	1.0	1.0
σ_e	0.3037	0.1743	0.1743	0.2638	0.1207	0.1207
σ_a	1.0	1.1606	0.3869	1.0	0.7292	1.2631
λ	0.057	0.0167	0.15	0.057	0.05	0.0167
ε	0.001	0.0001	0.001	0.001	0.0001	0.001
$\mu^{/}$	0.009	0.0037	0.0341	0.009	0.0112	0.0036
μ^{-}	0.033	0.0067	0.0614	0.033	0.0201	0.006
$\mu^{\backslash}$	0.015	0.0063	0.0614	0.015	0.0195	0.0062
θ		0.5	0.25		0.5	0.25

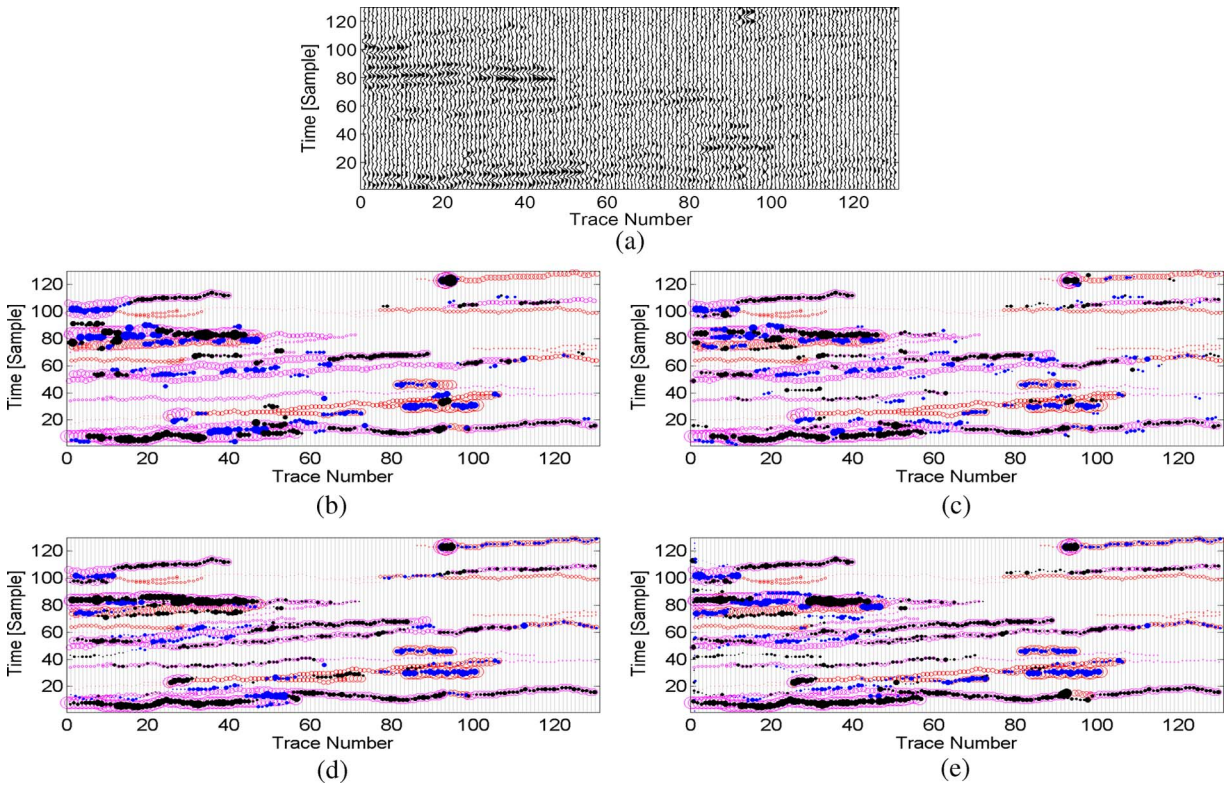

Fig. 6. Performances of MBD and IWM algorithms under medium SNR conditions (0 dB). True reflectivity appears as empty circles; red is for positive reflectors, and magenta is for negative ones. Estimated reflectivity appears as filled circles; blue is for positive reflectors, and black is for negative ones. The radius of the circles represents the magnitude of the reflectors. (a) Received traces. (b) and (c) Reflectivity estimates using IWM algorithm with different sparsity parameters. (d) and (e) Reflectivity estimate using MBD algorithm with different estimated model parameters.

reflectivity estimate, its probability might have decreased from the last iteration since the wavelet is different now. However, although the log probability might decrease between sequential iterations in the nonblind case, this rarely occurs, and the procedure still converges with similar convergence graphs.

F. Relation to Previous Work

In the SMLR approach [18], which is suited also for a single-channel deconvolution, the optimization criterion is maximized by a limited search, which tries to alter the current reflectivity by adding or removing a single reflector at a time. The approach presented in this paper is similar except that it tries to alter the reflectivity by adding or removing a complete legal path from the states set. Generally speaking, the search is among possible boundary sections' locations rather than among possible single reflectors' locations. The ability to search among boundary sections rather than among single reflectors without a significant complexity increase is due to the design of the states set so that legal paths well represent the typical structure of boundaries and the use of the Viterbi algorithm.

The iterated window maximization approach [5] takes into consideration the continuity of boundaries; however, it does so without a specific model. In addition, the account for continuity

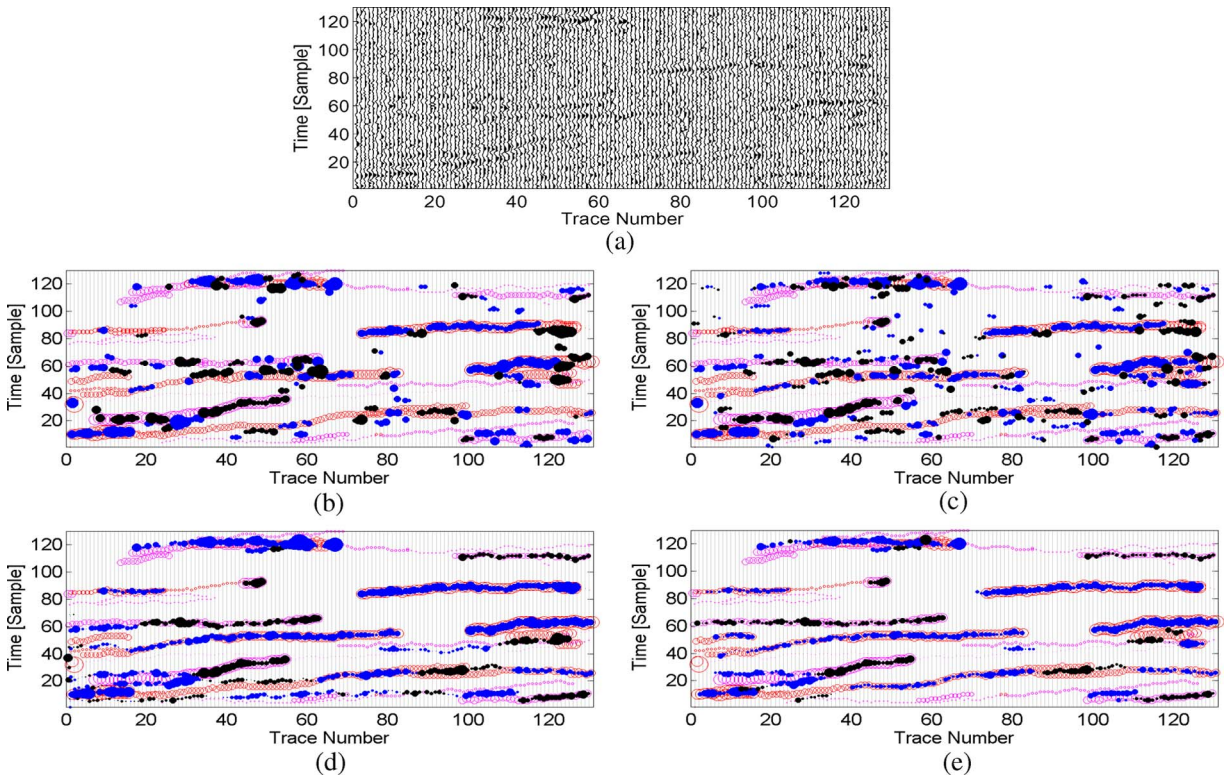

Fig. 7. Performances of the MBD and IWM algorithms under low SNR conditions (−5 dB). See Fig. 6 for explanation about the colors. (a) True reflectivity. (b) and (c) Reflectivity estimates using the IWM algorithm with different sparsity parameters. (d) and (e) Reflectivity estimates using the MBD algorithm with different estimated model parameters.

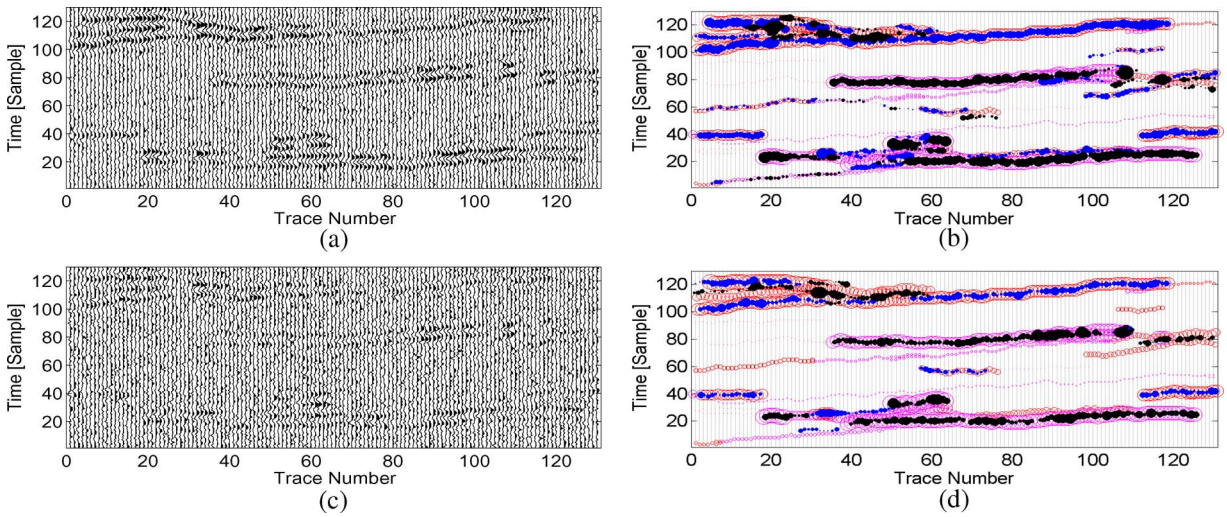

Fig. 8. Performances of the MBD algorithm in nonblind scenario under different SNR conditions (0 and −5 dB). See Fig. 6 for explanation about the colors. (a) Received traces with SNR of 0 dB. (b) Reflectivity estimate for 0 dB. (c) Received traces with SNR of −5 dB. (d) Reflectivity estimates for −5 dB.

is local; hence, the "relaxation" is slower in terms of the number of iterations, and also, many local optimum solutions are a cause for a suboptimal final estimate.

The algorithm of Idier and Goussard [17] and our algorithm are both based on a Markov–Bernoulli model. However, their optimization procedure is carried out in a suboptimal way. At the mth iteration, the reflectivity estimate of columns $1, \ldots, m-1$ is held fixed, and the reflectivity of the mth column is maximized with respect to the reflectivity of column $m-1$. Moreover, the columns to the right of the currently estimated column do not participate in the estimation. In the proposed approach, the estimate of a column is updated only after all columns were examined, and at each iteration, a truly global maximum of criterion (5) is found.

IV. Experimental Results

In the following sections, we present different results showing the performance of the proposed approach. In order to make it easy to compare the true reflectivity with the recovered one,

different colors are used as follows. The true reflectivity appears as empty circles; red is for positive reflectors, and magenta is for negative ones. The estimated reflectivity appears as filled circles; blue is for positive reflectors, and black is for negative ones. For both true and estimated reflectivities, the radius of the circles represents the magnitude of the reflectors.

A. Nonblind Procedure

Two sets of simulated 2-D reflectivity patterns of dimensions 130×130, were created according to the model described in Section II. The reflectivities are convolved with the wavelet shown in Fig. 4 and degraded by noise with -5- and 0-dB SNRs. The IWM algorithm of Kaaresen and Taxt and the proposed algorithm were applied to these data sets. The wavelet was considered known. Since the proposed algorithm employs the parameters of the signal model, these parameters should be given or estimated from the data. We have taken the following approach. The parameters λ and ε were assigned two different values in each of the two executions of the procedure. The noise variance was estimated as the variance of the samples in a 15×15 region with the smallest variance in the data. For each value of λ, the parameter σ_a was estimated as $\widehat{\sigma}_a = \sqrt{(\widehat{\sigma}_z^2 - \widehat{\sigma}_e^2)/\lambda}$. In the data, two pointers were chosen manually along the reflection from a distinct boundary. Such reflections can usually be observed even when the SNR is very low. Each point was selected so that it is the strongest for this reflection in its column. A simple dynamic programming algorithm was used to find the continuous path between the two selected pointers with the maximal absolute value of the sum of samples along it. This path is assumed to represent the typical direction of the boundaries in the data (since, usually, most boundaries have similar directions). From this path, the number of ascending, horizontal, and descending transitions were counted, and their relative probability was estimated. Using these results and the values of $\widehat{\lambda}$ and $\widehat{\varepsilon}$, the values of $\mu^{/}$, μ^{-}, and $\mu^{\backslash}$ were estimated. Fig. 5 shows some simulated data as a gray-level image; the region used to estimate the noise variance is marked with a black frame, and the two pointers and the path between them used to estimate $\mu^{/}$, μ^{-}, and $\mu^{\backslash}$ are shown with white and black dots, respectively. The value of r was set to one, both in the creation of the simulated data and in the algorithm. When the noise is high, this value has little effect since the true value is close to one and the variance in the estimated amplitude along a single boundary is mainly due to the estimate variance rather than due to the true change of amplitudes along the boundary.

For the IWM algorithm, two different values of the sparsity parameter θ were used in some reasonable range. Table II summarizes the true values of the parameters and the estimated values used by the algorithm for these simulations. Notice that, due to normalization of the observed data prior to the processing, the estimated values of σ_e and σ_a may be quite different from the true values. However, the important quantity is the ratio between them, which is more similar to the true value. The IWM algorithm was executed until it converged (no further changes occurred in the reflectivity estimate), and the proposed algorithm was stopped after 60 iterations. Figs. 6 and 7 show the results of applying the two algorithms to the two data sets. It can be seen that, for the higher noise example, the proposed algorithm recovers the 2-D reflectivity better than the competitive algorithm, whereas for the lower noise example, the results are only slightly better. Notice that the better performance of the proposed approach is not the result of an improper choice of a specific sparsity parameter for the competitive algorithm. Moreover, the results are almost the same for the two different sets of estimated parameters, which implies that the proposed algorithm is not sensitive to the values of the model parameters' estimates.

TABLE III
TRUE AND ESTIMATED VALUES OF PARAMETERS USED FOR NOISE EFFECT INVESTIGATION

	SNR 0dB:		SNR -5dB	
Parameter	True Value	Estimate	True Value	Estimate
r	1.0	1.0	1.0	1.0
σ_e	0.2414	0.1222	0.4294	0.1684
σ_a	1.0	0.7319	1.0	0.6112
λ	0.057	0.05	0.057	0.05
ε	0.001	0.0001	0.001	0.0001
$\mu^{/}$	0.009	0.01	0.009	0.0121
μ^{-}	0.033	0.0226	0.033	0.0184
$\mu^{\backslash}$	0.015	0.0181	0.015	0.0203

TABLE IV
TRUE AND ESTIMATED VALUES OF PARAMETERS USED FOR BLIND DECONVOLUTION EXAMPLES

		Blind Example:	SNR -5dB
Parameter	True Value		Estimates
		Execution: 1	2
r	1.0	1.0	1.0
σ_e	0.3037	0.1743	0.1743
σ_a	1.0	0.3869	0.6701
λ	0.057	0.15	0.05
ε	0.001	0.001	0.0001
$\mu^{/}$	0.009	0.0321	0.0112
μ^{-}	0.033	0.0642	0.0203
$\mu^{\backslash}$	0.015	0.0606	0.0193
θ		0.125	0.25

Influence of Noise: When the noise level is increased, the received data are less reliable, and the reflectivity model becomes more dominant. Less true reflectors are recovered, and more false reflectors appear. In addition, the estimation of the model parameters from the data is less accurate. However, the proposed algorithm exhibits good stability, in the sense that gradually increasing the amount of noise gradually degrades the results and does not cause sudden changes in the quality of the recovered reflectivity. This is shown in Fig. 8, where the nonblind procedure was applied for the same data with different noise levels (0 and -5 dB). It can be seen that the results are similar but that the recovered reflectivity for the lower noise is slightly better. The parameters used for these examples are displayed in Table III.

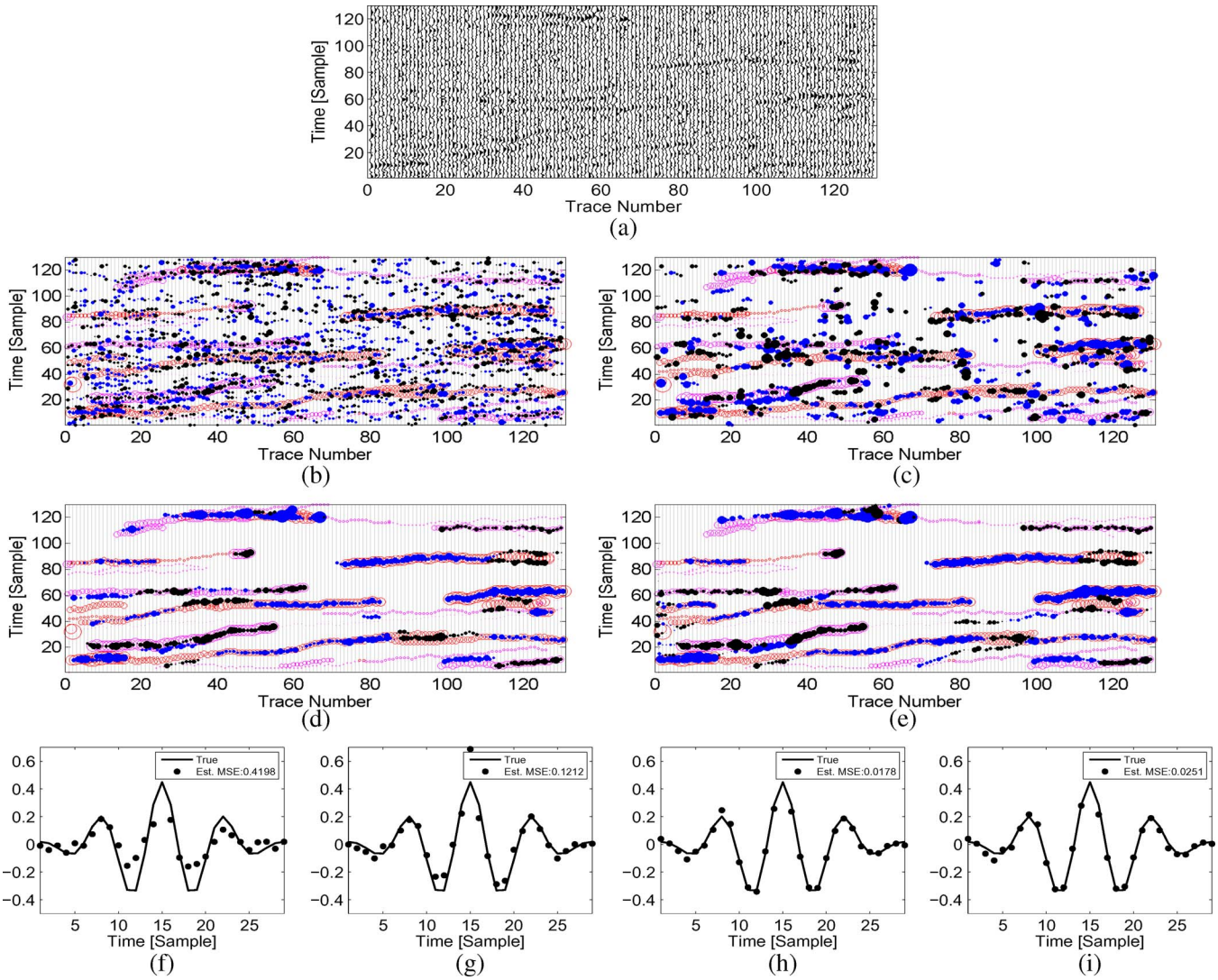

Fig. 9. Performances of the MBD and IWM algorithms in blind scenarios under low SNR conditions (−5 dB). See Fig. 6 for explanation about the colors. (a) True reflectivity. (b) and (c) Reflectivity estimates obtained by using the IWM algorithm with different sparsity parameters. (d) and (e) Reflectivity estimates obtained by using the MBD algorithm with different model parameters. (f)–(i) Wavelet estimates corresponding to (b)–(e).

B. Blind Procedure

In this example, the proposed and the competitive algorithms are applied to a blind problem. The observations used here are the same as those shown in Fig. 7. The wavelet is not given *a priori*. For the competitive algorithm, the procedure starts by some initialization of the reflectivity estimate based on strong points of local maximum in the data [5], then by alternately estimating the wavelet given the reflectivity, and then by estimating the reflectivity given the wavelet. For the proposed algorithm, the procedure starts by initializing the wavelet as a delta function, then, in a similar manner alternately, by estimating the reflectivity given the wavelet estimate, and then by estimating the wavelet given the reflectivity. In both algorithms, the estimate of the wavelet given the reflectivity is the least squares estimate, which is normalized to have a norm equal to one, to avoid the scale ambiguity between the recovered reflectivity and the estimated wavelet often encountered in blind deconvolution problems. The parameters of the proposed algorithm were estimated as described for the nonblind procedure. Table IV summarizes the true and estimated parameters' values used in this example for both executions.

Fig. 9 shows the results for the blind problem. Again, it can be seen that the proposed algorithm recovers the reflectivity better. Moreover, it can be seen that the wavelet estimate is characterized by a lower mean-squared error when using the proposed algorithm than the IWM algorithm.

C. Real Data Example

Fig. 10(a) shows real seismic data (courtesy of GeoEnergy Inc., Texas) containing 150 traces of 150 samples long. The estimated model parameters used for this example are displayed in Table V. The reflectivity and wavelet estimates obtained by using the IWM and proposed algorithms are shown in Fig. 10. Since the true layer structure is unknown, one can only appreciate the continuous nature of the channel estimates obtained by using the proposed algorithm.

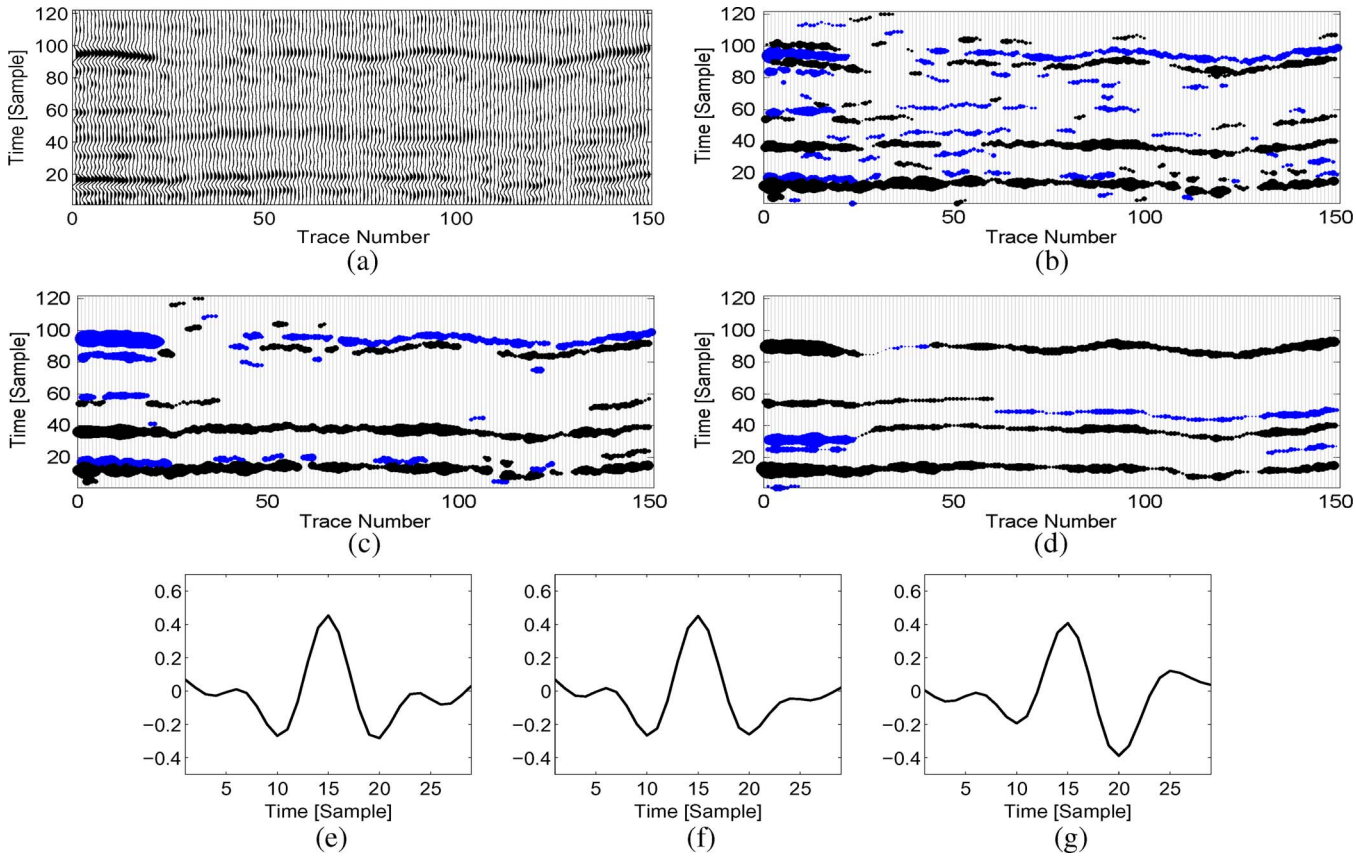

Fig. 10. Performances of the MBD and IWM algorithms in blind scenarios for real seismic data. See Fig. 6 for explanation about the colors. (a) Received traces. (b) and (c) Reflectivity estimates obtained by using the IWM algorithm with different sparsity parameters. (d) Reflectivity estimate obtained by using the MBD algorithm. (e)–(g) Wavelet estimates corresponding to (b)–(d).

TABLE V
ESTIMATED VALUES OF PARAMETERS USED FOR REAL DATA EXAMPLES

Parameter	MBD	IWM exe 1	IWM exe 2
r	1.0		
σ_e	0.2868		
σ_a	0.8409		
λ	0.05		
ε	0.0001		
$\mu^{/}$	0.0105		
μ^{-}	0.0286		
$\mu^{\backslash}$	0.0115		
θ		0.25	0.5

V. CONCLUSION

We have presented an algorithm for multichannel seismic deconvolution, which is based on Markov–Bernoulli random-field modeling of the lateral dependence between reflectors in consecutive traces. The computational complexity of the proposed algorithm is generally higher than that of the IWM algorithm. However, some reduction in complexity can be achieved by selecting, in each iteration, more than one path. Furthermore, when estimating the amplitudes for a new configuration of reflectors in a certain trace, not all the amplitudes need to be estimated, since reflectors that are distant from a newly added reflector or a removed reflector remain with nearly the same estimated amplitude values.

ACKNOWLEDGMENT

The authors would like to thank Dr. A. Vassiliou of GeoEnergy Inc., Houston, TX, for valuable discussions and helpful suggestions, and also the anonymous reviewers, for their constructive comments and suggestions.

REFERENCES

[1] A. J. Berkhout, "The seismic method in the search for oil and gas: Current techniques and future developments," *Proc. IEEE*, vol. 74, no. 8, pp. 1133–1159, Aug. 1986.
[2] C. B. Wason, J. L. Black, and G. A. King, "Seismic modeling and inversion," *Proc. IEEE*, vol. 72, no. 10, pp. 1385–1393, Oct. 1984.
[3] J. M. Mendel, J. Kormylo, F. Aminzadeh, and J. S. Lee, "A novel approach to seismic signal processing and modeling," *Geophysics*, vol. 46, no. 10, pp. 1398–1414, Oct. 1981.
[4] E. Baziw and T. J. Ulrych, "Principle phase decomposition: A new concept in blind seismic deconvolution," *IEEE Trans. Geosci. Remote Sens.*, vol. 44, no. 8, pp. 2271–2281, Aug. 2006.
[5] K. F. Kaaresen and T. Taxt, "Multichannel blind deconvolution of seismic signals," *Geophysics*, vol. 63, no. 6, pp. 2093–2107, Nov./Dec. 1998.
[6] I. Santamaria, C. J. Pantaleon, J. Ibanez, and A. Artez, "Deconvolution of seismic data using adaptive Gaussian mixtures," *IEEE Trans. Geosci. Remote Sens.*, vol. 37, no. 2, pp. 855–859, Mar. 1999.
[7] J. M. Mendel, "Tutorial on high-order statistics (spectra) in signal processing and system theory: Theoretical results and some applications," *Proc. IEEE*, vol. 79, no. 3, pp. 278–304, Mar. 1991.
[8] G. D. Lazear, "Mixed-phase wavelet estimation using fourth order cumulants," *Geophysics*, vol. 58, no. 7, pp. 1042–1051, Jul. 1993.
[9] A. Larue, J. I. Mars, and C. Jutten, "Frequency-domain blind deconvolution based on mutual information rate," *IEEE Trans. Signal Process.*, vol. 54, no. 5, pp. 1771–1781, May 2006.
[10] B. D. Jeffs, "Sparse inverse solution methods for signal and image processing applications," in *Proc. 23rd IEEE Int. Conf. Acoust. Speech Signal Process.*, May 1998, vol. 3, pp. 1885–1888.

[11] L. P. Meilhac, E. Moulines, K. A. Meraim, and P. Chevalier, "Blind identification of multipath channels: A parametric subspace approach," *IEEE Trans. Signal Process.*, vol. 49, no. 7, pp. 1468–1480, Jul. 2001.
[12] K. F. Kaaresen, "Evaluation and applications of the iterated window maximization method for sparse deconvolution," *IEEE Trans. Signal Process.*, vol. 46, no. 3, pp. 609–624, Mar. 1998.
[13] L. Tong and S. Perreau, "Multichannel blind identification: From subspace to maximum likelihood methods," *Proc. IEEE*, vol. 86, no. 10, pp. 1951–1968, Oct. 1998.
[14] G. Xu, H. Liu, L. Tong, and T. Kailath, "A least-squares approach to blind channel identification," *IEEE Trans. Signal Process.*, vol. 43, no. 12, pp. 2982–2993, Dec. 1995.
[15] H. Luo and Y. Li, "The application of blind channel identification techniques to prestack seismic deconvolution," *Proc. IEEE*, vol. 86, no. 10, pp. 2082–2089, Oct. 1998.
[16] M. Aurnhammer and K. D. Tonnies, "A genetic algorithm for automated horizon correlation across faults in seismic images," *IEEE Trans. Evol. Comput.*, vol. 9, no. 2, pp. 201–210, Apr. 2005.
[17] J. Idier and Y. Goussard, "Multichannel seismic deconvolution," *IEEE Trans. Geosci. Remote Sens.*, vol. 31, no. 5, pp. 961–979, Sep. 1993.
[18] J. J. Kormylo and J. M. Mendel, "Maximum likelihood detection and estimation of Bernoulli–Gaussian processes," *IEEE Trans. Inf. Theory*, vol. IT-28, no. 3, pp. 482–488, May 1982.
[19] M. Lavielle, "2-D Bayesian deconvolution," *Geophysics*, vol. 56, no. 12, pp. 2008–2018, Dec. 1991.
[20] A. Heimer, I. Cohen, and A. Vassiliou, "Dynamic programming for multichannel blind seismic deconvolution," in *Proc. 77th Annu. Meeting Soc. Exploration Geophysicist Int. Conf., Expo.*, San Antonio, TX, Sept. 23–28, 2007, pp. 1845–1849.
[21] A. Heimer and I. Cohen, "Multichannel blind seismic deconvolution using dynamic programming," *Signal Process.*, vol. 88, no. 7, pp. 1839–1851, Jul. 2008.
[22] D. G. Forney, "The Viterbi algorithm," *Proc. IEEE*, vol. 61, no. 3, pp. 268–278, Mar. 1973.
[23] J. Idier and Y. Goussard, "Markov modeling for Bayesian restoration of two-dimensional layered structure," *IEEE Trans. Inf. Theory*, vol. 39, no. 4, pp. 1356–1373, Jul. 1993.

Alon Heimer received the B.Sc. (*magna cum laude*) degree in electrical engineering from Ben-Gurion University, Beer-Sheva, Israel, in 2002, and the M.Sc. degree in electrical engineering from the Technion—Israel Institute of Technology, Haifa, Israel, in 2008.

Since 2003, he has been a Research Engineer with Electro-Optics Research and Development Company, Ltd., Technion City, Haifa. His research interests include array processing and system identification in applications of seismic and acoustic remote sensing.

Israel Cohen (M'01–SM'03) received the B.Sc. (*summa cum laude*), M.Sc., and Ph.D. degrees in electrical engineering from the Technion—Israel Institute of Technology, Haifa, Israel, in 1990, 1993, and 1998, respectively.

From 1990 to 1998, he was a Research Scientist with RAFAEL Research Laboratories, Israel Ministry of Defense, Haifa. From 1998 to 2001, he was a Postdoctoral Research Associate with the Computer Science Department, Yale University, New Haven, CT. Since 2001, he has been with the Department of Electrical Engineering, Technion, where he is currently an Associate Professor. His research interests include statistical signal processing; analysis and modeling of acoustic signals; speech enhancement; noise estimation; microphone arrays; source localization; blind source separation; system identification; and adaptive filtering. He was a Guest Editor of a special issue of the *EURASIP Journal on Advances in Signal Processing* on Advances in Multimicrophone Speech Processing and a special issue of the *EURASIP Speech Communication Journal* on Speech Enhancement. He is a Coeditor of the Multichannel Speech Processing section of the *Springer Handbook of Speech Processing* (New York, NY; Springer, 2007).

Dr. Cohen was the recipient, in 2005 and 2006, of the Technion Excellent Lecturer awards. He served as an Associate Editor of the IEEE TRANSACTIONS ON AUDIO, SPEECH, AND LANGUAGE PROCESSING and IEEE SIGNAL PROCESSING LETTERS.